We are IntechOpen, the world's leading publisher of Open Access books Built by scientists, for scientists

4,800
Open access books available

122,000
International authors and editors

135M
Downloads

Our authors are among the

154
Countries delivered to

TOP 1%
most cited scientists

12.2%
Contributors from top 500 universities

CLARIVATE ANALYTICS BOOK CITATION INDEX INDEXED

WEB OF SCIENCE™

Selection of our books indexed in the Book Citation Index in Web of Science™ Core Collection (BKCI)

Interested in publishing with us?
Contact book.department@intechopen.com

Numbers displayed above are based on latest data collected.
For more information visit www.intechopen.com

6

Wind Tunnel Testing of Pneumatic Artificial Muscles for Control Surface Actuation

Curt S. Kothera[1] and Norman M. Wereley[2]
[1]*Techno-Sciences, Inc.*
[2]*University of Maryland*
USA

1. Introduction

Control surfaces, such as trailing-edge flaps, provide a means to dynamically alter the aerodynamic characteristics of aircraft for primary flight control, secondary vibration control, and even higher frequency noise control. While the development of several novel technologies has been explored, many practical implementation barriers still exist for a single actuation system to serve all three of these objectives. This is particularly true for rotorcraft, where the demands of the harsh rotary and vibratory environment are severe in terms of actuator force and displacement, bandwidth limitations, life cycle concerns, and physical volume available. Accordingly, it has been assumed that on-blade active controls of a rotorcraft would be subject to the most stringent requirements in the subsonic flight regime, and if a control surface actuation technology could survive here, it could be reasonably applied to a fixed wing aircraft. A brief account of the current state-of-the-art for rotorcraft blade controls follows.

Helicopter rotors typically operate in a highly unsteady aerodynamic environment. In forward flight, the rotor blade sections experience large variations in angle-of-attack over one revolution. This is the primary source of performance degradation, such as high vibration and retreating blade stall. Actively changing the angle-of-attack of the blade sections as a function of blade azimuth has been shown to significantly alleviate vibration levels, as well as improve aerodynamic performance of the rotor (Straub et al., 2000). The change in angle-of-attack can be accomplished in a variety of ways. Implementation of high bandwidth hydraulic actuators in the rotating frame has demonstrated the ability to actively change the root pitch of the rotor blades and has since been demonstrated in both scale models (Lorber et al., 2001) and full scale tests (Arnold & Strecker, 2002). Another approach is to vary the aerodynamic forces on the blades by dynamically changing the geometry of the airfoil sections. This can be accomplished through actively controlling blade twist, airfoil camber, or through the use of trailing-edge flaps (Hall & Wereley, 1993). Recent advances in adaptive materials have led to a variety of schemes for on-blade actuation in these areas (Chopra, 2000). Some of these include piezoelectric innovations such as adaptive twist of the rotor blade (Chen & Chopra, 1997; Chen et al., 2001; Shin et al., 2005), trailing-edge flaps (Straub et al., 2001; Fulton, 2000; Fulton, 2005), and active camber control (Konstanzer et al., 2001; Nissly et al., 2005).

In comparing these approaches to active rotor systems, there are potential drawbacks, however. For instance, implementation of hydraulic systems in the rotating frame of

production helicopters is a challenging task due to the complexity of the system, the increase in maintenance associated with the large number of moving parts, as well as the hydraulic slip ring, and the added on-blade mass associated with the weight of the hydraulic fluid and piping. Considering the active blade twist concept, there is also a large weight penalty due to the distributed nature of the actuators. There are also several unanswered questions as to whether active material solutions like piezoelectrics can survive in the operational environment, whether they have sufficient fatigue life for practical consideration, or whether they are properly scaled for operating over broad deflection and frequency ranges in full size rotors. Despite this, there have been numerous developments aimed at demonstrating the potential that active materials have for full scale rotors. Most notable is the piezoelectric actuator work conducted independently by Boeing and Eurocopter. Both using piezoelectric actuators to drive trailing-edge flaps on rotor blades, the Boeing development led to full scale whirl testing for vibration control (Straub et al., 2004) and a full scale wind tunnel test for noise reduction (Straub et al., 2009), and the Eurocopter development led to full scale flight testing for vibration control (Roth et al., 2006; Dieterich et al., 2006).

Trailing-edge flaps provide localized actuation and can generate significant control authority, but these discrete control surfaces do increase drag from the discontinuities and abrupt changes in airfoil contour. The active camber control concept alleviates this issue by varying the camber of the airfoil to produce a conformal shape change. There are several technical barriers that exist in actual implementation, such as the development of a flexible skin and supporting core that can withstand the harsh rotating environment of a helicopter. These topics are beginning to be addressed in the fixed frame, such as in unmanned air vehicles (Flanagan et al., 2007; Bubert et al., 2010; Olympio & Gandhi, 2010), but the technology has not reached the maturity level required for rotorcraft. Therefore, it appears that the trailing-edge flap may be the leading candidate control scheme for active rotors given the current state-of-the-art in practical actuation strategies.

Using these drawbacks as motivation to investigate alternative approaches to active aerodynamic control, a less conventional, yet properly scalable, approach to trailing-edge flap actuation has been developed and tested, and it employs Pneumatic Artificial Muscles, or PAMs, as actuators (Kothera et al., 2010). These actuators, originally developed for orthotic devices in the 1950s by J.L. McKibben (Gaylord, 1958; Schulte, 1961), typically contract in response to an increase in internal pressure, and have been used in robotic applications (Tondu et al., 1994; Medrano-Cerda et al., 1995; Daerden & Lefeber, 2002). Typically constructed of an elastomeric bladder surrounded by a braided sleeve, the stroke in these low cost and light weight actuators comes from re-orientation of the stiff braid fibers as the bladder expands radially. Previous research with these devices has experimentally confirmed their applicability to trailing-edge flaps in both the fixed frame (Woods et al., 2007; Kothera et al., 2008; Woods et al., 2010a) and the rotating frame (Bubert et al., 2007; Woods et al., 2010b). The development of and results from these fixed-frame tests will be presented here from two different mechanical configurations and loading conditions, as a step toward demonstrating the feasibility of using PAM actuators for aerospace applications. The next section will discuss the general system design, which will be followed by a discussion of bench-top testing results. Then the wind tunnel test article development is shown, along with experimental test data.

2. System design

Three different PAM actuation systems were designed, built, and tested, with experimental evaluations taking place first on the bench and then moving on to a wind tunnel. In each case, the aerodynamic hinge moment was predicted first and then the design of the actuation mechanism followed.

2.1 Aerodynamic prediction

The actuation system design used two-dimensional thin airfoil theory to predict the hinge moments that were used in sizing the actuators and bench-test loading springs to simulate the aerodynamic hinge moments. Environmental parameters used in the calculations are those of Sea Level Standard (SLS), which have a temperature of T = 288 K, pressure of P = 101.3 kPa, and air density of ρ = 1.225 kg/m^3. The maximum speed of the Glenn L. Martin wind tunnel (GLMWT) at the University of Maryland is Mach 0.3, so this was also used in the design as a maximum free-stream condition, and a reasonable angle-of-attack of $\alpha = 6^o$ was also incorporated. It was assumed in this loading mechanism design that there was no flow separation over the airfoil and that the gap between the flap and the airfoil was sealed.
The most important quantity for prediction in terms of sizing the actuation system is the hinge moment. This can be calculated according to

$$c_h = c_{h\alpha}\alpha + c_{hf}$$
$$H = \frac{1}{2}\rho v^2 S_f c_f c_h,$$

where c_h is the hinge moment coefficient, $c_{h\alpha}$ is the hinge coefficient due to angle-of-attack, c_{hf} is the hinge coefficient due to flap deflection, H is the actual hinge moment, v is the wind speed, S_f is the flap area, and c_f is the chord of the flap. For the angle-of-attack effects, tabulated airfoil data can be used with the equation

$$c_{h\alpha} = \left(b_1\right)_0^* + 2\left[\left(a_1\right)_{0T}^* - \left(a_1\right)_0^*\right]\tan\left(0.5\tau - t/c\right),$$

where (b_1) is the rate of change of hinge moment coefficient with incidence, the (a_1) terms are related to the lift-curve slope, τ is the trailing-edge angle, and t/c is the thickness ratio (Etkin, 1982). The effect on the hinge moment due to flap deflection is computed by

$$c_{hf} = \frac{dc_h}{dc_l}c_l + \frac{dc_h}{d\delta}\delta,$$

where dc_h/dc_l is the rate of change of the hinge moment coefficient with respect to the change in lift coefficient, $dc_h/d\delta$ is the rate of change of the hinge moment coefficient with respect to the change in flap deflection, c_l is the lift coefficient, and δ is the flap deflection (Abbott & von Doenhoff, 1959). Because this term depends on the lift coefficient, its computation was also required in the prediction. For the current case with a flap on the trailing-edge, added lifting effects from the flap on the lift coefficient can be approximated as

$$c_l = c_{l\alpha}\left(\alpha + k\delta\right),$$

where k is the fraction for how the flap deflection angle changes the effective angle-of-attack of the airfoil (Eastman & Pinkerton, 1930). Here, the lift coefficient due to angle-of-attack is estimated with Mach scaling according to

$$c_{l\alpha} = \frac{2\pi}{\sqrt{1-M^2}},$$

where M is the Mach number. The denominator in this equation is commonly denoted as the parameter β.

As was mentioned, a total of three PAM-flap systems were evaluated. Table 1 lists the key design parameters for each and defines each with a "system number," which will be used throughout to more easily identify the results being shown. As can be seen, all three systems were sized for NACA 0012 airfoils with nominal angles-of-attack of 6 degrees. It should also be noted that each successive system was designed and tested for a higher Mach number. The first two systems were identical in terms of the overall model size and flap size, with the second containing stronger PAM actuators for the higher air loads. The third system was designed for an even higher wind speed and a smaller airfoil section to better illustrate the capability of the PAM actuators for scalability and high performance.

System No.	1	2	3
Wind Speed (M)	0.1	0.3	0.56
Angle-of-Attack (deg)	6	6	6
Airfoil Type	NACA 0012	NACA 0012	NACA 0012
Airfoil Chord (in)	21	21	10.5
Flap Chord (in)	3.15	3.15	1.61
Flap Span (in)	10	10	34

Table 1. Details of specific trailing-edge flap systems

Using the aerodynamic equations listed above with the airfoil specifics and wind speeds in Table 1 led to predictions of the hinge moments that would need to be generated by the PAM actuation systems to deflect the various flaps. Figure 1 displays the simulation results for the noted systems and conditions. In each set of results, the estimated, bi-directional hinge moment contributions are shown from the airfoil angle-of-attack (green) and the flap deflection (red), along with the summed total (blue). Figure 1(a) shows the hinge moment for system 1 at the design condition, Figure 1(b) shows the hinge moment for system 2 at the design condition, and Figure 1(c) shows the hinge moment for system 3 at the design condition. Figure 1(d) has also been included to estimate the wind tunnel test condition for system 3. While designed for Mach 0.56, the test facility has a maximum wind speed of only Mach 0.3, so the designed actuation system was bench tested to the full spring-simulated aerodynamic stiffness, but it was wind tunnel tested to a reduced load with input pressure scaled accordingly. In order to meet the goal of at least 10 degrees of flap deflection, the PAM actuators must be able to produce 2.2 in-lb, 23 in-lb, and 70 in-lb for the noted design conditions of systems 1 – 3, respectively. Being that system 3 would be designed for operating at Mach 0.56, it would have little trouble meeting the reduced hinge moment requirement of only 22 in-lb for the wind tunnel test.

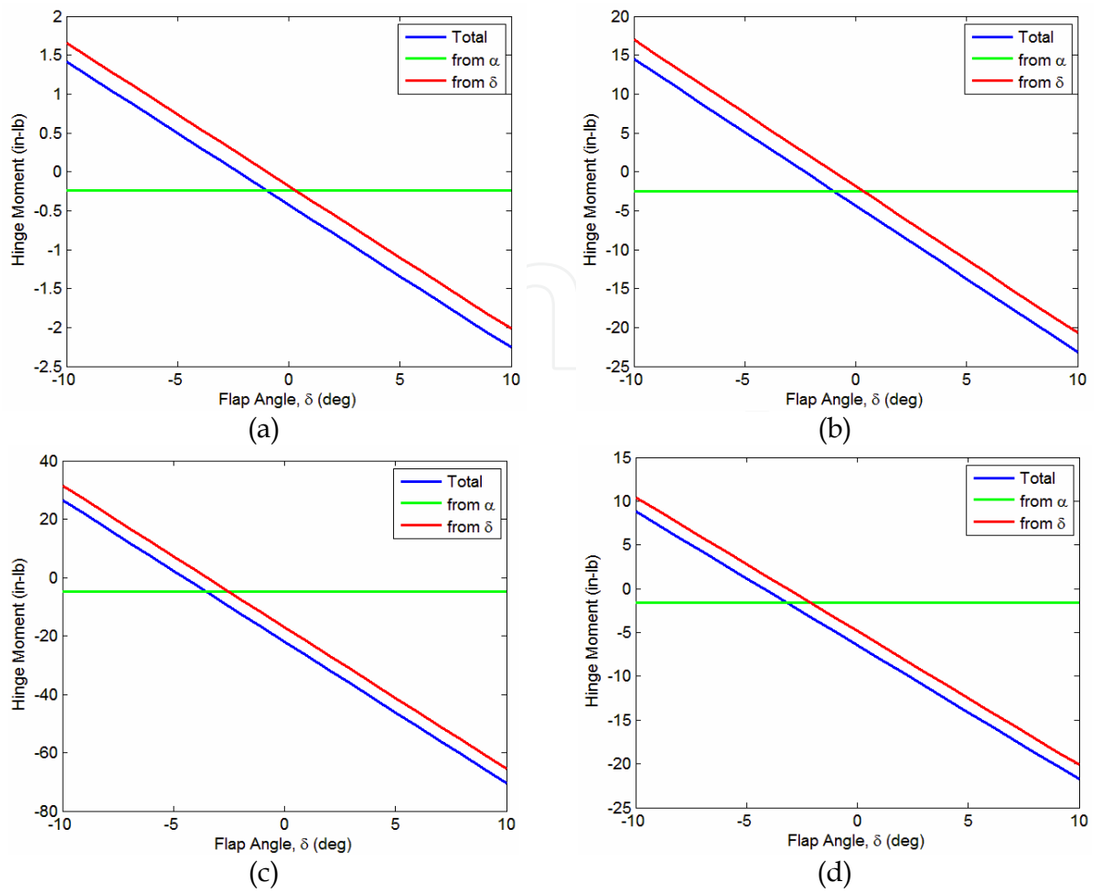

Fig. 1. Hinge moment predictions for actuation system designs – (a) system 1; (b) system 2; (c) system 3 bench-top; (d) system 3 wind tunnel

2.2 Actuator design

For the most part, the PAM actuation systems were sized to fit entirely within the airfoil contour. A schematic diagram of how the PAM system functions is provided in Figure 2. In this figure, the upper PAM is inactive (open to atmosphere, $P_1 = 0$) and the lower PAM is active (pressurized, $P_2 > 0$). The basic operation of a PAM actuator is to produce a contractile stroke upon internal pressurization. This stroke is the result of radial expansion of the elastomeric bladder, which is surrounded by a double helical weave of stiff fibers (e.g., polyethylene terephthalate - PET). As the softer bladder expands, the stiff fibers maintain their length and reorient themselves to accommodate the radial expansion. Consequently, the length of the device decreases. Also as indicated in the figure, any time pressure in one of the PAMs exceeds that in the other antagonistic PAM, a moment is generated about the flap hinge. The case shown is $P_1 < P_2$, which causes the flap to deflect in the downward direction.

There are two key equations for predicting the deflections of the antagonistic PAM actuation system. The first is the arc length formula

$$\frac{\Delta L}{r} = \frac{L_1 - L_2}{r} = \delta,$$

where L_1 is the length of the inactive PAM, L_2 is the length of the active PAM, and r is the hinge radius. These are all labeled in Figure 2 with the convention that downward flap deflection angles are positive and upward flap deflection angles are negative.

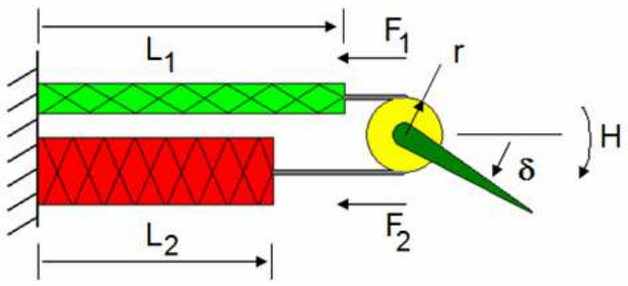

Fig. 2. Diagram of bi-directional PAM-flap actuator

The second equation considers the available actuation force by

$$\Delta F = F_2 - F_1 = \frac{H}{r},$$

where F_1 is the inactive PAM force (e.g., at 0 psi), F_2 is the active PAM force, and H is the hinge moment generated on the flap. For bi-directional operation of the flap, an antagonistic actuator arrangement is typically preferred.

Based on these actuator design equations and the aerodynamic hinge moment predictions from section 2.1, an in-house database of PAM actuator performance data was consulted to select the actuator characteristics best suited to each of the three systems. Table 2 displays the results of this actuator sizing analysis. For the first two systems, which are essentially the same except for the increased strength of the second, a chordwise PAM orientation was selected. This means that the length and stroke direction of the PAM actuators is along the airfoil chord, which was made possible by the large airfoil section (21-in chord). System 3 could not use chordwise actuators because of the higher forces required and the smaller size of the airfoil section. In this case, a spanwise orientation was selected, whereby the spanwise pulling motion of the PAM actuators is transferred into chordwise motion to deflect the flap through the use of a kinematic mechanism. While adding complexity and increasing the part count, having a mechanism does allow for consideration of mechanical advantage trade-offs to better tune system performance. For instance, when comparing the system 2 and 3 actuators, it can be seen that larger diameter PAMs were used for system 2 although the expected loads were smaller here than for system 3. Note that it is a general design rule for PAMs with the same braid angle that larger diameter actuators will produce more force for a given pressure. This use of smaller diameter PAMs of essentially the same braid angle was facilitated by the mechanism, where stroke could be traded for force. As indicated in the table, the PAMs for system 3 are over 9 inches long, whereas the PAMs for system 2 are just over 3 inches in active length.

Force-contraction data was collected from experiments conducted on a servo-hydraulic load frame. For each case, the PAM actuator was installed in the machine at its resting length, as shown in Figure 3(a). Next, the noted pressure was applied and held constant throughout the test. Immediately after the pressure was applied, the actuator blocked force measurement was recorded. Then, the actuator was allowed to contract slowly, or quasi-statically, to the point where no force was measured. This point is known as the free

System No.	1	2	3
Orientation	Chordwise	Chordwise	Spanwise
No. PAM Pairs	1	2	1
Diameter (in)	0.5	1.0	0.625
Active Length (in)	3.15	3.15	9.10
Resting Braid Angle (deg)	47	60	61
Braid Material	PET	PET	Kevlar
Bladder Material	Latex	Latex	Latex
Mechanical Advantage	1	1	1.15

Table 2. Details of specific PAM actuators selected for system designs

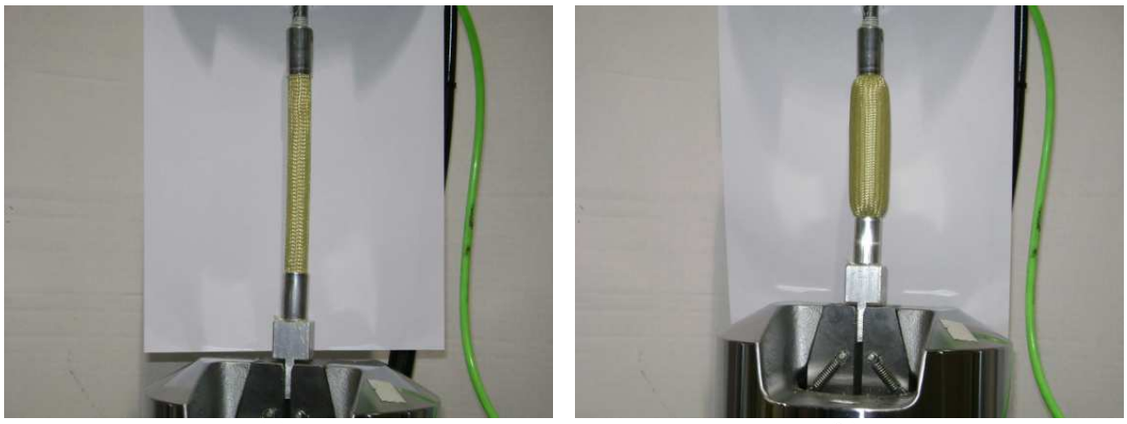

(a) (b)

Fig. 3. Characterization testing of PAM actuator – (a) resting length; (b) free contraction

contraction value and is shown in Figute 3(b). After recording this value, the PAM actuator was stretched back to its resting length and the test was stopped. Typical performance data from each of the three selected PAM configurations is provided in Figure 4 at various pressure settings. Note that the x-axis data is presented as the non-dimensional contraction percentage. For the range of PAM lengths considered in this work, it has been shown that contraction percentage is largely independent of PAM length for a given diameter and braid angle. As an example, a particular PAM at a given pressure may have a free contraction of 25%. This actuator with a 4-in resting length would thereby have a free contraction of 1 inch, whereas a 12-in resting length actuator would have a free contraction of 3 inches.

It can be seen in Figure 4 that both force and contraction increase with pressure. For the performance metric of blocked force (measured force with 0% contraction, i.e., resting length and maximum possible force), the increase in force is linear with pressure, but the same is not true for the performance metric of free contraction (measured contraction with 0 lb force, i.e., maximum possible stroke). The free contraction increases with pressure, but tends to roll off as a maximum limit is approached. These trends are valid, of course, only over the pressure range which does not lead to yield in the braid fibres. It should be noted here that our tests have shown that the PET braid does not begin to yield until approximately 200 psi and the yield point for the Kevlar braid is over 1000 psi. Given that the three system designs here are all intended to operate below 100 psi, a more than adequate safety margin exists for burst failure. Another characteristic to mention in regard to the typical force-contraction

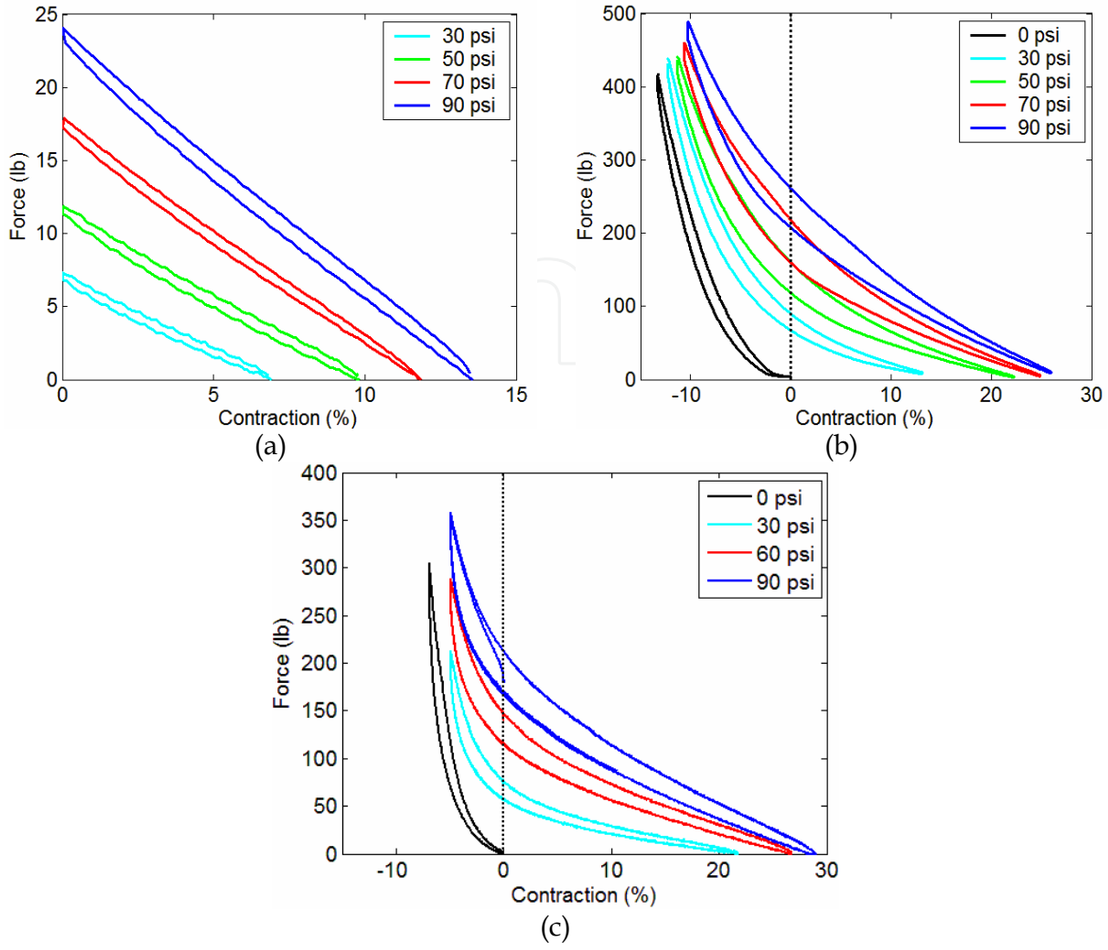

Fig. 4. Performance data from PAM actuators selected for system designs – (a) system 1; (b) system 2; (c) system 3

behaviour of PAM actuators is that some measure of hysteresis does exist in the loop. Despite the noticeable hysteresis, average values and a linear force-contraction approximation between blocked force and free contraction may be sufficient for initial system design and component sizing exercises. To state the maximum values of blocked force and free contraction (at 90 psi) for the system 1 – 3 actuators, respectively, we have 24 lb with 14%, 250 lb with 27%, and 200 lb with 29%.

3. Bench-top testing & validation

3.1 Experimental setup

To evaluate the PAM trailing-edge flap actuation systems prior to entering a wind tunnel environment, each of the three actuation systems was tested on a laboratory bench. Figure 5 shows the test setups that were designed, fabricated, and tested. First in Figure 5(a) is a system sized for low subsonic air loads with the single pair of antagonistic PAM actuators (system 1) oriented along the chord of the airfoil. Here, the compressed air enters and exits the PAM actuators from their end near the upper-right corner of the photograph. Two aluminum extensions are at their other end and are instrumented with resistive strain gages

for measurement purposes. Representative inertia is mounted on the axis of flap rotation and a bending spring is attached to simulate aerodynamic stiffness. Figure 5(b) shows a similar arrangement with chord-oriented PAM actuators, but this system has two antagonistic pairs of larger PAM actuators (system 2) to increase the quasi-static flap deflection output. It can be seen in the figure that the PAMs attach to the hinge from one side and a spring loading mechanism attaches to the hinge axis from the other side. Linear extension springs were used for this test. Figure 5(c) shows an antagonistic pair of PAM actuators intended for spanwise orientation in the airfoil section, which uses a mechanism (not pictured) to turn the actuator work into chordwise motion that rotates the flap about its hinge axis (system 3). An inertial element was attached to the top of the axis of rotation here and linear extension springs were connected at a different radius than the PAMs to account for the mechanism that would be installed in the airfoil section. Also note that the difference in physical appearance of the PAMs from system 1 and 2 (black) to those in system 3 (yellow) is due to the use of a different braid material.

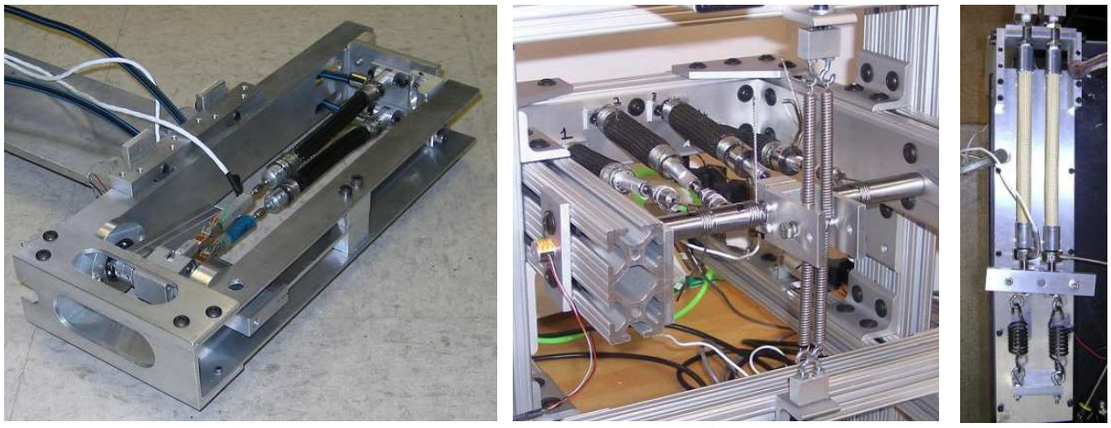

(a) (b) (c)

Fig. 5. Experimental setups for bench-top evaluations – (a) system 1; (b) system 2; (c) system 3

For each of the three test cases, the hinge rotation angle was measured with a Hall-effect angle sensor (Midori, series QPC). Two of the PAM actuators were instrumented with load cells (Honeywell) and the actuation pressure was measured with a pressure transducer (Omega, series PX209). Solenoid valves were used to direct the air flow into and out of the PAMs, as directed by a square wave voltage input for these open-loop experiments. For the two chordwise PAM configurations, the control valves used were SMC model VZ solenoids and for the spanwise PAM configuration, it was a Festo model MPYE valve with a much higher flow capacity. A National Instruments data acquisition system and laptop computer were used to run the experiments and to collect data. The test procedure included driving the control valves at various input frequencies and under different spring loads to measure the dynamic response of the PAM actuation systems in terms of flap deflection angle bandwidth.

3.2 Bench-top test results

Figure 6 shows the bench-top test results from the three cases as half peak-to-peak deflection values that were averaged over several actuation cycles. Here, Figure 6(a) shows data from system 1 for a range of pressures. It should be noted that the spring load indicated in the caption simulates air loads existing at a free-stream velocity of Mach 0.23, while the design

condition was only for Mach 0.1. The difference here was due to spring availability at the time of the test, so a more conservative loading condition (approximately four times the expected wind tunnel load) was tested on the bench-top. Given that the PAM actuation system was able to produce nearly ±5 degrees of flap deflection over the tested frequency range of 30 Hz provided sufficient assurance that the system would meet, and most likely surpass, the ±10 degree target in the wind tunnel. As expected from basic PAM operation, this figure also shows that increasing the pressure led to increased deflection capability. Figure 6(b) shows data from the Mach 0.3 spring load of the chordwise, double PAM pair actuators (system 2) at various pressures, showing a different characteristic than was shown for system 1. As can be seen, the quasi-static deflection output increases fairly linearly with actuation pressure, but there is a sharp roll-off in deflection performance at frequencies above 1 Hz that reduces the achievable deflection level at higher frequencies. Additionally, the measured deflection at high frequency appears to be independent of pressure. These response features indicate that air flow restrictions were present in the pneumatic supply system. This is a reasonable outcome when considering that the same pneumatic valves were used for systems 1 and 2, while the air volume required for operating system 2 was much larger than that for system 1. This was later improved upon in a revised bench-

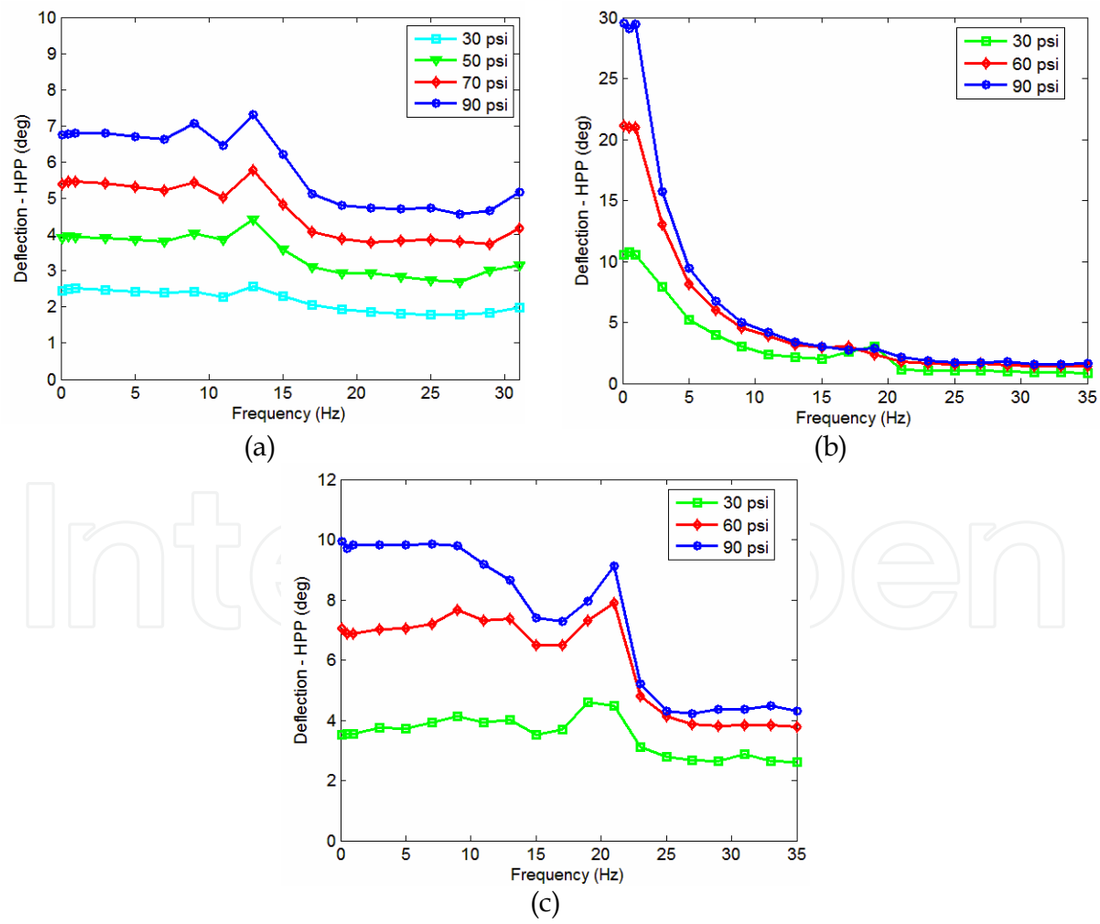

Fig. 6. Bench-top test results – (a) system 1 with Mach 0.23 spring load; (b) system 2 with Mach 0.3 spring load; (c) system 3 with Mach 0.56 spring load

top test, but the improved pneumatics for system 2 was not tested in a wind tunnel, so those results will not be presented here (Kothera et al., 2008). In continued scaling of the PAM actuation system, system 3 did incorporate improved pneumatic elements. Figure 6(c) shows experimental flap deflection measurements from a Mach 0.56 spring load at various pressures for system 3, where it can be seen that the deflection bandwidth was significantly increased over that seen from system 2, with ±10 degrees now being produced up to nearly 10 Hz at 90 psi. Based on these results, it was concluded that systems 1 and 3 would meet the goal of at least ±10 degrees of flap deflection in the dynamic response for their respective wind tunnel tests, but system 2 would likely fall short of the goal due to the flow rate restrictions in the pneumatic circuit. These tests also verified proper basic functionality of the actuation systems.

4. Wind tunnel testing

After successful bench-top evaluations, the trailing-edge flap actuation systems were placed in various wind tunnel test articles to assess their performance under actual aerodynamic loading conditions. This section will discuss the test article fabrication and experimental test results.

4.1 Wind tunnel test article development

The three PAM actuation systems were integrated into different test articles based on their originally specified performance conditions and measured performance from the bench-top evaluations. Systems 1 and 2 had the same geometry, as stated in Table 1, but different construction was used to better match the test conditions. That is, system 2 was designed with a stronger frame structure and skin than system 1. The frame for system 1 was constructed with 0.25-in aluminum and consisted of a spar running the span of the airfoil section (24-in), an airfoil-shaped end plate at both ends, and two intermediate support ribs that extended from the spar to the trailing-edge. The flap hinge was fabricated from a precision ground 0.25-in stainless steel rod, and the flap was able to rotate about the hinge with a bearing at each end. The skin was made with a wet lay-up process using two plies of pre-impregnated fibreglass, and formed the shape of the airfoil section with a Styrofoam mold. Additional reinforcement at the leading-edge was provided with a thin sandwich structure of fibreglass and foam, which formed a shell-like structure around the spar so that the solenoid valves and air tubing could be installed inside. The system 2 wind tunnel model had the same basic layout as the system 1 model, but it was made to be stronger since it was to be tested at Mach 0.3. That is, it had two airfoil-shaped end plates and two mid-span support ribs, all constructed of 0.5-in aluminum, and a steel spar. The entire skin was also fabricated as sections of sandwich structure composites with foam core inside 2-ply fibreglass. There was a separate leading-edge, or D-spar section, and aft panels that were fastened to the frame structure. As with system 1, system 2 also placed the solenoid control valves inside the D-spar cavity surrounded by the shell-like skin. Figure 7(a) shows the system 1 wind tunnel model installed in the test fixture between two acrylic vertical walls and positioned in front of the free-jet wind tunnel. Figure 7(b) shows the wind tunnel model for system 2, which was fixed at the floor of the Glenn L. Martin wind tunnel at the University of Maryland and cantilevered upward. There was also an elliptical top plate bolted to the top of the cantilevered model to promote more desirable air flow characteristics over the test section. The primary difference in appearance of these two models is that the system 1 model was left bare and the system 2 model was painted black. Note also that strips of aluminum tape were placed over the recessed fasteners.

The wind tunnel model for system 3 was fabricated with an entirely different approach than those for systems 1 and 2. In this case, instead of building the complete airfoil section from raw materials, the outboard section of a scrapped full-scale Bell 407 helicopter rotor blade was employed as the basis for the wind tunnel model. Since this rotor blade does not currently feature a trailing-edge flap, the blade was physically modified to accept a flap and the PAM actuation system. The spanwise PAM actuators and mechanism were mounted inside the D-spar of the blade and the aft section of the blade was removed. This section was first used to create a mold for the new trailing-edge flap so that the geometry of the blade could be matched exactly. Note that the production Bell 407 blade contains taper and twist, which would have otherwise been difficult to match in constructing the flap. Aluminum strips were bonded inside the remaining aft portion of the blade skin where the flap section had been removed in order to provide bearing surfaces and structural support to fasten the trailing-edge flap in place. The flap was supported at the inboard and outboard ends and at two intermediate locations. A hole was drilled in the aft wall of the spar and a slot was placed in the skin to attach a control rod from the mechanism inside the spar to a control horn on the trailing-edge flap. These parts are on the opposite side of blade section in Figure 7(c), so they are not visible in the photograph; the control rod was located at the inboard edge of the flap, or near the floor in the figure. Recall that system 3 was the only system for which a component of the PAM actuation system violated the baseline airfoil profile. This was due largely to the smaller size of the airfoil section and the higher wind loading condition. Also note that the tip of the cantilevered blade section was laterally restrained with a cable to limit side-to-side motion of the blade during flap actuation.

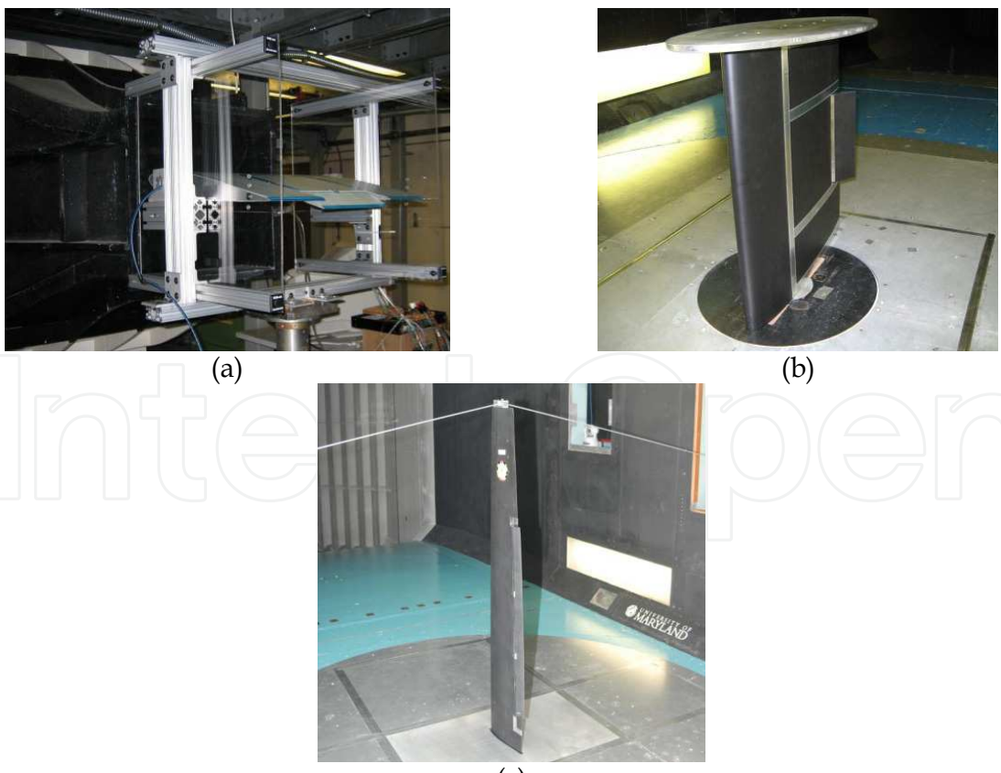

Fig. 7. Wind tunnel test articles – (a) system 1, free-jet; (b) system 2, closed-circuit; (c) system 3, closed-circuit

4.2 Wind tunnel test results

Test results in the form of averaged, half peak-to-peak deflection are displayed in Figure 8, following the same layout as the previous figures. Shown in each case are the measured results from the previously specified wind tunnel test conditions, with the effect of varying actuation pressure also displayed for systems 1 and 3. Reaching a maximum speed of Mach 0.1, Figure 8(a) shows the open-loop dynamic response of system 1 at various actuation frequencies and pressures. As was inferred from the bench-top test, this PAM actuation system was able to far exceed the original goal of ±10 degrees at high frequency. At only 30 psi operating pressure in the PAMs, this system was able to produce ±10 degrees beyond 20 Hz, and operating the PAM actuators with 90 psi led to ±20 degrees of flap deflection being produced up to nearly 25 Hz. There is also a resonance phenomenon apparent in this data set, which can be seen to increase in frequency with pressure. This changing resonance frequency is attributed to the changing stiffness of the PAM actuators as their operational pressure changes. Figure 8(b) shows the experimental flap deflections from system 2 that were measured at 90 psi in the PAM actuators and at two different angles-of-attack, though there is little noticeable difference in the dynamic response of the system at the two angles-of-attack.

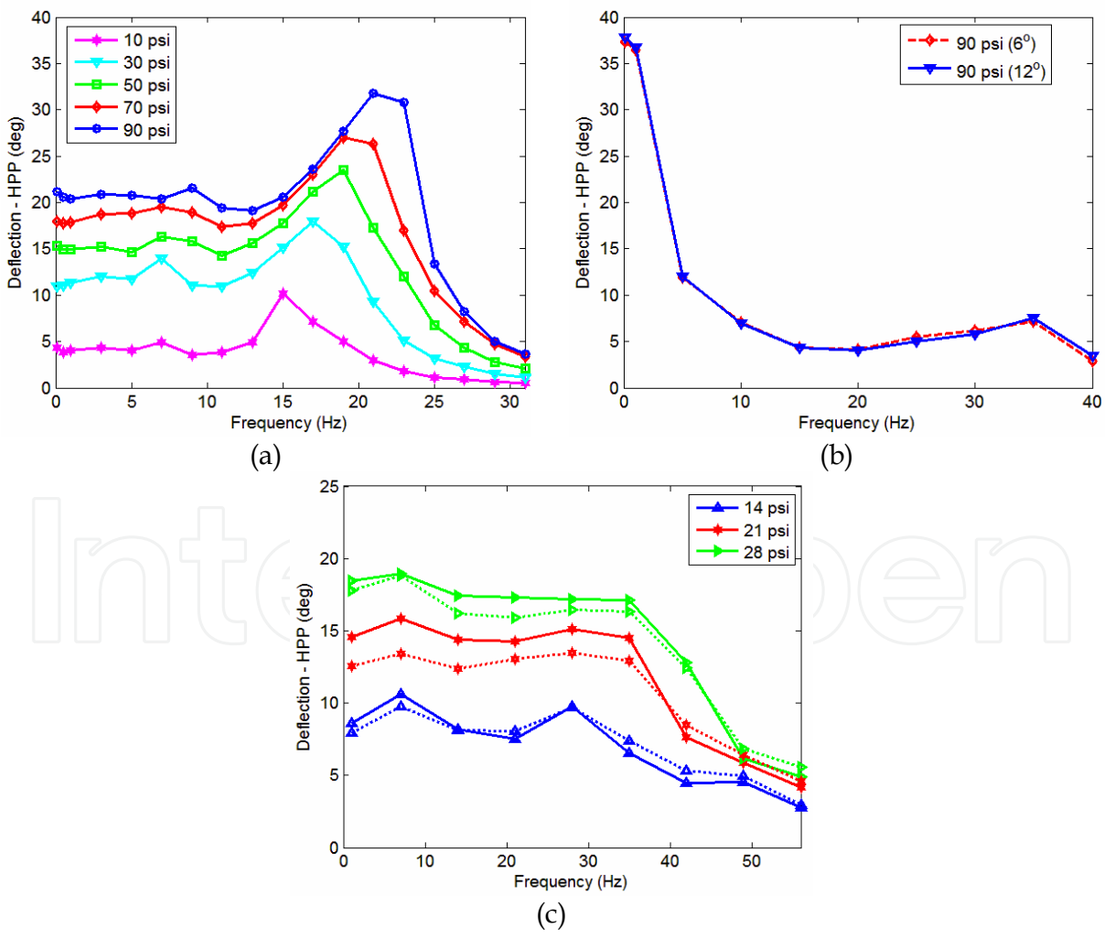

Fig. 8. Wind tunnel test results – (a) single PAM pair, chordwise at Mach 0.1; (b) double PAM pair, chordwise at Mach 0.3; (c) single PAM pair, spanwise at Mach 0.3

As was expected from the bench-top test results, this system again illustrates a rapid drop off in achievable flap deflection as the actuation frequency increases. Recall that this was due to flow limitations in the pneumatic components. The ability to produce almost ±40 degrees quasi-statically at Mach 0.3, however, is a promising result for the technology, especially when the dynamic response shown can be viewed as potentially a worst case situation achieving ±4 degrees of flap deflection up to 40 Hz.

Figure 8(c) shows the wind tunnel results for system 3 at Mach 0.3. Recall that this is reduced from the bench-top test condition (Mach 0.56), but was the maximum possible speed of the wind tunnel used for testing. There are also two lines for each of the noted actuation pressure levels. The solid line represents the flap deflection measured at the inboard edge of the flap and the dotted line represents the deflection at the outboard edge of the flap. Since there is some difference between the two ends of the flap, this implies that there was some wash-out present in the model. This could be reduced in the future by increasing the torsional stiffness of the trailing-edge flap or attaching the actuation mechanism to a more central location on the flap instead of at the inboard end. Regardless of this effect, the measured actuation performance met and exceeded the goal of ±10 degrees dynamically. Nearly 10 degrees can be maintained for up to 30 Hz at only 14 psi PAM operating pressure, whereas nearly 18 degrees can be maintained for up to 35 Hz when driving the PAM actuators with 28 psi. Recall that this test case is a reduced load from the expected condition, so the PAM input pressures had to be reduced, as well. Based on all of these results, it can be stated that PAM actuation systems have clearly demonstrated their high performance capabilities for aerospace applications.

5. Conclusion

This research has developed and tested a series of innovative trailing-edge flap actuation systems that exploit antagonistic configurations of Pneumatic Artificial Muscles (PAMs) to generate bi-directional flap deflections. The systems were designed and built for experimental evaluation on the bench-top under simulated aerodynamic loadings with spring mechanisms and in the wind tunnel under actual aerodynamic conditions up to the maximum speed (Mach 0.3) of the Glenn L. Martin wind tunnel at the University of Maryland. Results showed that the flap deflection range produced was attractive to various flight control regimes, including flight control, vibration control, and even noise control. The key conclusion of this work is that PAM actuation systems have demonstrated the ability to dynamically control large flap deflections over a wide bandwidth in these varying control regimes and offer an attractive solution to aerodynamic control applications.

6. Acknowledgments

This research and development was conducted under several SBIR projects sponsored by the Army. Specifically contract number W911W6-05-C-0007 (technical monitors Drs. Tin-Chee Wong and John D. Berry), contract number W911W6-06-C-0033 (technical monitor Dr. Mark V. Fulton), and contract number W911W6-07-C-0053 (technical monitor Dr. Mark V. Fulton). The authors greatly appreciate this support. The authors would also like to acknowledge the effort and contributions made by Prof. Jayant Sirohi, Mr. Benjamin K.S. Woods, Mr. Edward A. Bubert, Mr. Robert D. Vocke, and Mr. Shane M. Boyer.

7. References

Abbott, I.H. and von Doenhoff, A.E. (1959). *Theory of Wing Sections*, Dover Publications, New York.

Arnold, U.T.P. and Strecker, G. (2002). Certification, ground and flight testing of an experimental IBC system for the CH-53G helicopter, *Proceedings of American Helicopter Society 58th Annual Forum*, ISBN, Montreal, Quebec, June 2002.

Bubert, E.A., Woods, B.K.S., Sirohi, J., Kothera, C.S., and Wereley, N.M. (2007). Whirl Testing of Pneumatic Artificial Muscle Systems for Helicopter Rotor Applications, *Proceedings of ASME International Design Engineering Technical Conference*, Las Vegas, NV, September 2007.

Bubert, E.A., Woods, B.K.S., Lee, K., Kothera, C.S., and Wereley, N.M. (2010). Design and Fabrication of a Passive 1D Morphing Aircraft Skin, *Journal of Intelligent Material Systems and Structures*, Vol. 21 (November 2010) pp. 1699-1717.

Chen, P.C. and Chopra, I. (1997). Wind Tunnel Test of a Smart Rotor Model With Individual Blade Twist Control, *Journal of Intelligent Material Systems and Structures*, Vol. 8 (May 1997) pp. 414-425.

Chen, P.C., Baeder, J.D., Evans, R., and Niemczuk, J. (2001). Blade-Vortex Noise Reduction with Active Twist Smart Rotor Technology, *Journal of Smart Materials and Structures*, Vol. 10 (January 2001) pp. 77 – 83.

Chopra, I. (2000). Status of application of smart structures technology to rotorcraft systems, *Journal of the American Helicopter Society*, Vol. 45 (October 2000) pp. 228-252.

Daerden, F. and Lefeber, D. (2002). Pneumatic Artificial Muscles: actuators for robotics and automation, *European Journal of Mechanical and Environmental Engineering*, Vol. 47 (January 2001) pp. 10 – 21.

Dieterich, O., Enenkl, B., and Roth, D. (2006). Trailing Edge Flaps for Active Rotor Control Aeroelastic Characteristics of the ADASYS Rotor System," *Proceedings of the American Helicopter Society Annual Forum*, Phoenix, AZ, May 2006.

Eastman, J.N. and Pinkerton, R.M. (1930). Pressure Distribution Over a Symmetrical Airfoil Section with Trailing Edge Flap, In: *NACA Technical Report No. 360*, NACA Digital Library.

Etkin, B. (1982). *Dynamics of Flight*, 2nd ed., Wiley Publications, New York.

Flanagan, J.S., Strutzenberg, R.C., Myers, R.B., and Rodrian, J.E. (2007). Development and Flight Testing of a Morphing Aircraft, the NextGen MFX-1, *Proceedings of AIAA Structures, Structural Dynamics and Materials Conference*, Honolulu, HI, April 2007.

Fulton, M.V. (2000). Design of the Active Elevon Rotor for Low Vibration, *Proceedings of American Helicopter Society Aeromechanics Specialists Meeting*, Atlanta, GA, November 2000.

Fulton, M.V. (2005). Aeromechanics of the Active Elevon Rotor, *Proceedings of American Helicopter Society 61st Annual Forum*, Grapevine, TX, June 2005.

Gaylord, R. (1958). Fluid actuated motor system and stroking device, United States Patent No. 2,844,126.

Hall, S.R. and Wereley, N.M. (1993). Performance of higher harmonic control algorithms for helicopter vibration reduction, *AIAA Journal of Guidance, Control and Dynamics*, Vol. 16 (Jul-Aug 1993) pp. 794-797.

Konstanzer, P., Grohmann, B., and Kroplin, B. (2001). Decentralized Vibration Control and Coupled Aeroservoelastic Simulation of Helicopter Rotor Blades with adaptive Airfoils, *Journal of Intelligent Material Systems and Structures*, Vol. 12 (April 2001) pp. 209 – 214.

Kothera, C.S., Wereley, N.M., Woods, B.K.S., and Bubert, E.A. (2008). Wind Tunnel Testing of a Trailing-Edge Flap Actuated by Pneumatic Artificial Muscles, *Proceedings of American Helicopter Society 64th Annual Forum*, Montreal, Quebec, April 2008.

Kothera, C.S., Woods, B.K.S., Sirohi, J., Wereley, N.M., and Chen, P.C. (2010). Fluid-driven artificial muscles as mechanisms for controlled actuation, United States Patent No. 7,837,144.

Lorber, P., Park, C., Polak, D., O'Neill, J., and Welsh, W.A. (2001). Active rotor experiments at Mach scale using root pitch IBC, *Proceedings of American Helicopter Society 57th Annual Forum*, ISBN, Washington DC, May 2001.

Medrano-Cerda, G.A., Bowler, C.J., and Caldwell, D.G. (1995). Adaptive position control of antagonistic pneumatic muscle actuators, *Proceedings of IEEE Intelligent Robots and Systems Conference*, Vol. 1 (1995) pp. 378 – 383.

Nissly, A., Anusonti-Inthra, P., Gandhi, F., and Frecker, M. (2005). Design Optimization of a Controllable Camber Rotor Airfoil, *Proceedings of American Helicopter Society 61st Annual Forum*, Grapevine, TX, June 2005.

Olympio, K.R. and Gandhi, F. (2010). Flexible Skins for Morphing Aircraft Using Cellular Honeycomb Cores, *Journal of Intelligent Material Systems and Structures*, Vol. 21 (November 2010) pp. 1719-1735.

Roth, D., Enenkl, B., and Dieterich, O. (2006). Active Rotor Control by Flaps for Vibration Reduction – Full scale demonstrator and first flight test results, *Proceedings of the European Rotorcraft Forum*, Maastricht, Netherlands, September 2006.

Schulte, H.F. (1961). The characteristics of the McKibben artificial muscle, *In: The Application of External Power in Prosthetics and Orthotics*, *Publication 874*, National Academy of Sciences – National Research Council, Washington DC, App. H, pp. 94 – 115.

Shin, S.J., Cesnik, C.E.S., and Hall, S.R. (2005). Closed-loop control test of the NASA/Army/MIT active twist rotor for vibration reduction, *Journal of the American Helicopter Society*, Vol. 50 (April 2005) pp. 178-194.

Straub, F.K., Ngo, H.T., Anand, V., and Domzalski, D.B. (2001). Development of a piezoelectric actuator for trailing edge flap control of full scale rotor blades, *Smart Materials and Structures*, Vol. 10 (2001) pp. 25 – 34.

Straub, F.K., Kenedy, D.K., Stemple, A.D., Anand, V.R., and Birchette, T.S. (2004). Development and whirl tower test of the SMART active flap rotor, *Proceedings of SPIE Symposium on Smart Structures and Materials*, San Diego, CA, March 2004.

Straub, F.K., Anand, V.R., Birchette, T.S., and Lau, B.H. (2009). Wind Tunnel Test of the SMART Active Flap Rotor, *Proceedings of the American Helicopter Society Annual Forum*, Grapevine, TX, May 2009.

Tondu, B., Boitier, V., and Lopez, P. (1994). Naturally compliant robot-arms actuated by McKibben artificial muscles, *Proceedings of IEEE Conference on Systems, Man, and Cybernetics*, Vol. 3 (October 1994) pp. 2635 – 2640.

Woods, B.K.S., Bubert, E.A., Kothera, C.S., Sirohi, J., and Wereley, N.M. (2007). Experimental Testing of Pneumatic Artificial Muscles for Trailing-Edge Flap Actuation, *Proceedings of AIAA Structures, Structural Dynamics and Materials Conference*, Waikiki, HI, April 2007.

Woods, B.K.S., Kothera, C.S., and Wereley, N.M. (2010a). Whirl Testing of a Pneumatic Artificial Muscle Actuation System for a Full-Scale Active Rotor, *Proceedings of American Helicopter Society 68th Annual Forum*, Phoenix, AZ, May 2010.

Woods, B.K.S., Wereley, N.M., and Kothera, C.S. (2010b). Wind Tunnel Test of a Helicopter Rotor Trailing Edge Flap Actuated via Pneumatic Artificial Muscles, *Proceeding of ASME Conference on Smart Materials, Adaptive Structures and Intelligent Systems*, Philadelphia, PA, September 2010.

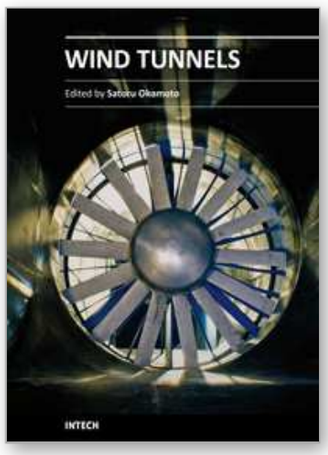

Wind Tunnels

Edited by Prof. Satoru Okamoto

ISBN 978-953-307-295-1

Hard cover, 136 pages

Publisher InTech

Published online 10, February, 2011

Published in print edition February, 2011

Although great advances in computational methods have been made in recent years, wind tunnel tests remain essential for obtaining the full range of data required to guide detailed design decisions for various practical engineering problems. This book collects original and innovative research studies on recent applications in wind tunnel tests, exhibiting various investigation directions and providing a birdâ€™s eye view on this broad subject area. It is composed of seven chapters that have been grouped in two major parts. The first part of the book (chapters 1â€“4) deals with wind tunnel technologies and devices. The second part (chapters 5â€“7) deals with the latest applications of wind tunnel testing. The text is addressed not only to researchers but also to professional engineers, engineering lecturers, and students seeking to gain better understanding of the current status of wind tunnels.ã€€Through its seven chapters, the reader will have an access to a wide range of works related to wind tunnel testing.

InTech Europe

University Campus STeP Ri
Slavka Krautzeka 83/A
51000 Rijeka, Croatia
Phone: +385 (51) 770 447
Fax: +385 (51) 686 166
www.intechopen.com

InTech China

Unit 405, Office Block, Hotel Equatorial Shanghai
No.65, Yan An Road (West), Shanghai, 200040, China
中国上海市延安西路65号上海国际贵都大饭店办公楼405单元
Phone: +86-21-62489820
Fax: +86-21-62489821

IntechOpen